Memristive Effects in Nanopatterned Permalloy Kagomé Array

W.B.J. Fonseca,[1] F. Garcia,[1] F. Caravelli,[2] and C.I.L. de Araujo[3,*]

[1] *Centro Brasileiro de Pesquisas Físicas, Rio de Janeiro, Brazil*

[2] *Theoretical Division (T4), Los Alamos National Laboratory, Los Alamos, New Mexico 87545, USA*

[3] *Departamento de Fìsica, Laboratório de Spintrônica e Nanomagnetismo, Universidade Federal de Viçosa, Viçosa, Minas Gerais 36570-900, Brazil*

(Received 25 October 2021; revised 30 May 2022; accepted 1 July 2022; published 27 July 2022)

We study memristive effects in kagomé nanopatterned permalloy. We observe that at low frequencies a thermistor effect is present, a phenomenon arising due to the lithography and absent in similar experiments for thin films. However, we also show via an independent anisotropic magnetoresistive study that a small hysteresis accounting for 1% of the effect is not attributable to a thermistive effect. Such an effect is also confirmed by a careful subtraction scheme between nearby thermal hysteresis. In the millihertz regime, an effective model is provided to describe the experimental results for the thermistor, showing that there should be a crossover from the millihertz to the gigahertz, from a thermistor to a memristive effect for nanopatterned permalloy.

DOI: 10.1103/PhysRevApplied.18.014070

I. INTRODUCTION

In the last decade we witnessed an increasing interest in artificial physical systems, obtained via nanopatterning magnetic materials, as for instance artificial spin ice [1–5]. It is now possible, via recent techniques in lithographic printing, to think of tailor-designed magnetic materials addressing old and future technological applications [6–16]. The purpose of this paper is to provide theoretical and experimental evidence for the particular application of such tailor-designed materials to magnetic induced resistive memory. Moreover, spin ice materials can be directly used for computing purposes [17–20]. Memory effects in resistive materials can be used for a variety of computing applications including logical gates [21–24], unconventional computing [25–30], or machine learning [31–34].

A possible pathway towards the implementation of current-controllable dynamical memory in an artificial magnetic material is via the use of anisotropic magnetoresistance (AMR) in symbiosis with many-body magnetic effects; this possibility is backed up both by recent experimental studies [35–37] and theoretical ones [38,39]. Instead of using disconnected magnetic nanoislands, one can focus on connected magnetic nanowires, which we assume to have a resistance per unit of length ρ_0.

In a recent paper [39] it has been noted that the interplay between the magnetization of the permalloy and the AMR can lead to a memory effect reminiscent of the one of a memristor. Such a study was also backed up recently in a tailored analysis of nanorings [40]. It is thus worth exploring other mechanisms leading to similar effects in patterned magnetic devices. However, realistic devices have all sorts of effects to consider, and this paper focuses on permalloy heterostructures.

A memristor is a device that satisfies Ohm's law $V = R\,I$, but moreover has a dynamical resistance of the form $dR/dt = f\,(R, I)$ (or alternatively defined in terms of the voltage). Because Ohm's law is still valid, any memory effect due to the current history in the device must still be such that to zero applied voltage there is no current leak from the device. Such a requirement excludes capacitance or inductance at the first order of approximation. For instance, the Strukov-Williams memristor, initially discovered while studying titanium dioxide [41], can be approximated (far from the resistive boundaries) by the functional form

$$\frac{dR}{dt} = \beta I - \gamma R + \eta, R_{\rm on} \leq R(t) \leq R_{\rm off}. \qquad (1)$$

The equation above is the one of a switch, e.g., a device that changes its resistive state between two values $R_{\rm on} \ll R_{\rm off}$. Such a functional form has been fitted theoretically to the memristors introduced in Ref. [39], under the assumption of spinlike islands of an artificial spin ice. The mechanism, which induced the memristor feedback in the artificial spin ice (ASI) approximation, was a current-induced domain-wall formation, which is well documented in the literature [42–45]. However, real magnetic materials

*dearaujo@ufv.br

have complicated dynamical behavior of the magnetization, many-body effects not captured by a simple Ising-like variable, interaction with the current captured by the Zhang-Li coupling [46], and temperature effects that can be attributed to thermistors [47].

In the present paper we provide theoretical, numerical, and experimental evidence that both temperature-induced and possibly magnetic memory is present in nanopatterned magnetic devices. In the first part of this work we discuss the experimental results and then discuss how the thermal effect can explain the low-frequency regimes measured in experiments. The last part of the paper is concerned with micromagnetic simulations of these samples in the high-frequency regimes. Conclusions follow.

II. EXPERIMENTS AND METHODS

A. Sample preparation

For the experimental verification of the memristance in nanostructured samples, we develop kagomé lattices by colloidal nanolithography. The process [summarized in Fig. 1(a)] consists of transferring floating monolayers of self-assembled (hexagonal closely packed) polystyrene spheres (PS), at air-water interface, to a 300-nm thermally oxidized silicon substrate [48,49]. Then, to increase the spacing between the PS spheres, the monolayers are developed by reactive ion etching with oxygen plasma for 12.5 min.

After this first step, a magnetic material deposition process is performed with 20-nm permalloy thin film capped by 3 nm of platinum, deposited by sputtering over the set of substrates, plus PS spheres' mask. Finally, the PS spheres are removed by deionized water ultrasonic bath to yield kagomé lattices. Figures 1(b) and 1(c) show scanning electron microscopy images of a representative lattice among the grown kagomé lattices, using spheres with 1 μm and 500 nm diameter, respectively.

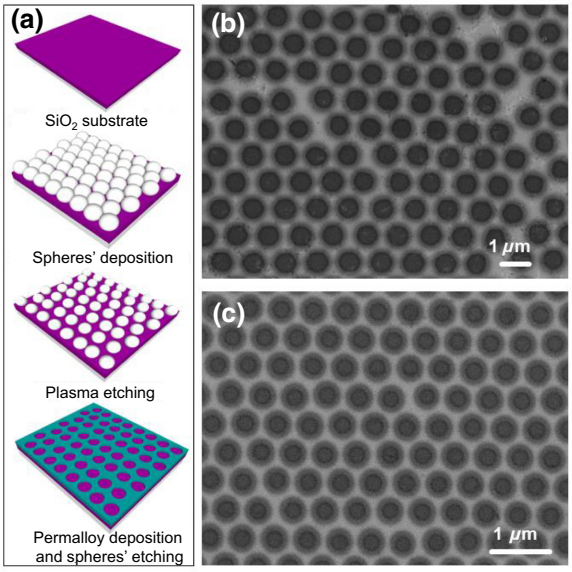

FIG. 1. Colloidal lithography of the sample. We show in (a) silicon substrate with a 300-nm thermal oxide layer, polysthyrene spheres' distribution after deposition by drop casting and solution dry, spheres' diameter decrease by corrosion with oxygen plasma etching, and 20-nm Py/3nm Pt sputtering and liftoff. Scanning electron microscopy shows the kagomé lattices obtained by using spheres of diameter (b) 1 μm and better quality when spheres of diameter (c) 500 nm are used.

B. Hysteretic magnetoresistance

In order to perform electric and magnetoresistive characterization of our samples, 50-nm gold electric contacts, preceded by 3 nm chrome electric contacts for better adhesion, are developed by sputtering in the geometries depicted in Fig. 2.

To investigate the magnetoresistive behavior we perform measurements in the longitudinal configuration [Fig. 2(a)], with an angle of $\theta = 0$ between the applied current and sweep external magnetic field direction, and in the transverse configuration [Fig. 2(b)] with $\theta = 90$. Our

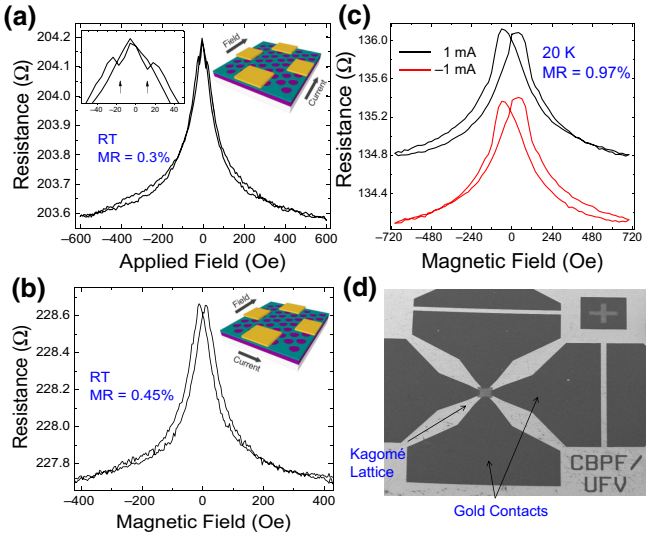

FIG. 2. AMR experiment to show hysteresis in the sample. (a) Magnetoresistance measured at room temperature in longitudinal configuration represented in the sketch. The anisotropic behavior highlighted in the inset is suppressed by the effect of magnetization vertex, owing to a magnetoresistance signal of 0.3%. (b) Magnetoresistance measured at room temperature in transverse configuration represented in the sketch with a magnetoresistance signal of 0.45%: here the anisotropic signal is summed with the vertex magnetization effect. (c) Longitudinal magnetoresistance performed at T = 20 K, showing broadening of the magnetoresistive peak and better observation of hysteresis asymmetry in the curve shape as a function of applied current direction. (d) Image of the electrical contacts utilized.

results on the magnetoresistive effect are in accordance with those present in the literature [35]. The anisotropic effect expected due to spin-orbit coupling in the permalloy thin film, highlighted in the inset of Fig. 2(a), is extremely suppressed by the dynamics of the vertex magnetization, which are responsible for the isotropic behavior observed in Figs. 2(a) and 2(b), performed at room temperature.

It is worthwhile to point out that the colloidal nanolithography we utilize has allowed an increase in the vertex size, in comparison with the nanowires' width. As a result, the magnetoresistive effect we measure is approximately 2 orders of magnitude bigger than the ones observed in electron-beam nanolithography samples of previous experiments [35]. Moreover, we observe in the magnetoresistive curves an even more pronounced signal in the measurements performed at T = 20 K, as presented in Fig. 2(c). Hysteresis asymmetries are also observed in the curve shape for positive and negative external fields, depending on the current signal, and in the resistance for positive and negative applied currents. This suggests that there is both the AMR effect and a pinched hysteresis in the resistivity, providing evidence of a memory effect as previously predicted [35,39].

C. Memristance

To test whether the resistive memory is memristive in nature, we perform a typical experiment to characterize the resistive hysteresis. In this experiment, electrical characterization is performed in order to observe a memory effect, e.g., a splitting of the resistive typical I-V curve in two branches. For this purpose, a Keithley 2400 sourcemeter is used to apply cycles of linear dc currents, while pinched hysteresis in voltage is observed in the systems, and the obtained results are shown in Fig. 3. Specifically, since the kagomé wires' resistance are higher than those of the contacts, we are able to perform the high scalable two-point probe $I \times V$ measurements, in order to investigate the resistive memory effect in our samples with currents up to 100 mA, applied in samples at room temperature and at $T = 20$ K.

The results presented in Fig. 3(a), both for a continuous permalloy thin film and kagomé lattice of 1-μm-diameter spheres performed at room temperature and T = 20 K, clearly show the memristive phenomenon characterized by the typical pinched loop in the $I \times V$ curve plot. Such an effect increases as temperature decreases, following the same behavior observed in the magnetoresistive curves. In the continuous permalloy thin film, one can see that resistance is very low in comparison with the kagomé sample and just a very short loop in $I \times V$ measurement is observed, in comparison with nanowired samples (kagomé) (3(a) inset).

In order to check whether the memristive hysteresis is a function of the frequency and of the external applied

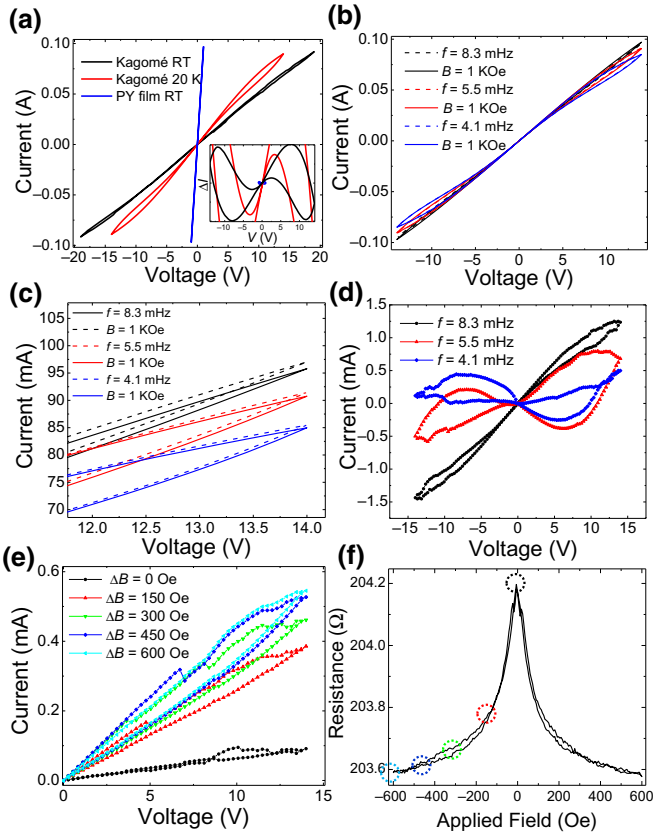

FIG. 3. (a) $I \times V$ curves performed at room temperature and at T = 20 K for kagomé lattices and at room temperature for permalloy thin film (residual linear fit in the inset), (b) $I \times V$ curves at T = 20 K with different frequencies and under an external magnetic field of 1000 Oe, (c) Enlarged view of the difference for the curves with and without magnetic field, (d) curves obtained from the difference between measurements performed with and without external field, (e) difference between measurements performed at intermediate fields, and (f) magnetoresistance (MR) curve with marks in the fields utilized for the memristive curves in (e).

magnetic field, we perform the same hysteresis experiment in the $I \times V$ curve measurements described earlier. This time, however, using a different waiting time for the points' acquisition with and without external magnetic field. As we show in Fig. 3(b), the memory effect is higher for long $I \times V$ curve acquisition (4.1 mHz). This behavior is also typical in commercial or other sorts of memristive devices. Figure 3(c) shows an increase in the dependence of the effect with external magnetic field as a function of acquisition time.

In all the $I \times V$ measurements performed with and without an external field, the predicted resistive hysteresis is present. We notice however memristive signals up to 13%, much larger than that expected from the analysis of Ref. [35], which considers just effects coming from many-body magnetization flips, that should be in the same magnitude of sample AMR 1%.

In Fig. 3(d) we plot instead the difference between the hysteresis curves, when the samples are submitted to a field strong enough to saturate the nanowire and vertice magnetization, for the different frequencies measured. Such a plot is carried out in order to remove the part of signal probably coming from thermal effects, which also contributes to possible effects coming from magnetization dynamics, leaving just the many-body effect. After the subtraction of the two curves obtained with and without magnetization saturation by external field, the characteristic pinched hysteresis loop is observed, now with the same magnitude of 1%. In Fig. 3(e) we present similar curves for the measurements performed under intermediate fields. A very small cycle-to-cycle variation is observed (black curve), while under successive applied field memristive effect is increased up to saturation around 600 Oe. The proportionality of the memristive signal with the resistive change under external field can be noticed in the magnetoresistive curve presented in Fig. 3(f).

D. Thermocouple analysis

Because of the disparity between the AMR measurement and the observed resistance change, the bulk of the memristive effect has to be found elsewhere. It was already demonstrated in the literature that persistent high currents needed to move the domain walls in such permalloy nanowires, in same order of 1×10^{12} A/m^2 utilized in the present work, could be able to increase the temperature up to 800 K [50] in nanowires with similar geometries to those utilized in our samples. Such temperatures could be high enough to stimulate thermal fluctuations of magnetization [51].

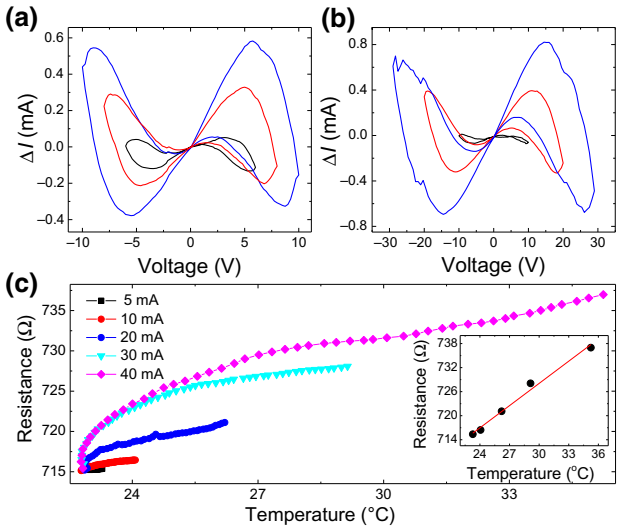

FIG. 4. Residual linear fit of the $I \times V$ curve performed with different applied voltages in a kagomé lattice from spheres of (a) 0.5 μm and (b) 1 μm. (c) Sample resistance and temperature variation as a function of different currents applied for a 50-s interval.

An insight of the thermal effects' relevance in the high memristive signal measured can be obtained from the measurements performed in samples with different nanowire lengths presented in Fig. 4. The resistance measured in a sample obtained with 500-nm-diameter spheres [Fig. 4(a)] is half of the sample resistance obtained with 1-μm spheres [Fig. 4(b)], which presents higher memristive effects with the same applied current of 100 mA.

To map the evolution of resistance as a function of sample heating by the Joule effect, we apply different persistent currents and measure the evolution of sample temperature with a K-type thermocouple for the 50-s, timescale similar to the utilized for the $I \times V$ curves. Results presented in Fig. 4(c) show the linear evolution of resistance of around 0.54Ω per Celsius degree.

The difference between the curves of Fig. 4(c), and the hysteretic AMR analysis previously discussed, show that a temperature-based memristor model alone cannot explain all the effects in the material.

III. THEORETICAL ANALYSIS OF TEMPERATURE CONTRIBUTIONS

A. Thermistor effect in heterostructures

While the splitting of the AMR experiment confirms a spin-transfer torque effect, at the Hertz frequency we still have an effect of the temperature on the resistivity, causing a memristive hysteresis [47]. It is worthwhile to characterize here the properties of this thermistor in our samples. Let us assume that the resistivity of the material changes with the temperature, and that moreover we are in the regime of a thermistor. We thus ignore for the moment the AMR effect, e.g., a temperature-dependent resistor with conductance $R(T)$. We want to show here that such an effect is relevant because of the nanopatterning, which is consistent with the experimental results, due to the difference in area between a thin film and a heterostructure.

In order to explain this effect we use a thermistor model [47] for the material. This is given by

$$V(t) = R(w_T)I(t), \tag{2}$$

$$R(w_T) = R_0\Big(1 + T_r\alpha_T(w - w_0)\Big), \tag{3}$$

$$\frac{dw_T}{dt} = \frac{V(t)^2}{\tau_v\bar{v}^2[1 + T_r\alpha_T(w_T - w_0)]} - \frac{1}{\tau}(w_T - 1), \tag{4}$$

where T_r is room temperature, and for permalloy we have $\alpha T_r \approx 1/3$. The parameter w_T physically represents the internal temperature of the permalloy. The parameter R_0 is fit to be approximately 720Ω for our device at room temperature. The parameter $\tau \approx 1 - 10$ s and represents the thermalization time of the sample at room temperature.

Then, Ohm's law for the effective resistance of the sample follows

$$V(t) = R_{\text{eff}}(t, T)i(t). \tag{5}$$

The sample can dissipate energy both through the silicon substrate and via radiative transfer. If δ is the conduction per unit of area, σ the Stefan-Boltzmann constant, and c the heat capacity of the material, we have

$$\begin{aligned} C\frac{dT}{dt} &= i(t)v(t) - A\Big(\delta(T - T_0) + \sigma(T^4 - T_0^4)\Big) \\ &= i(t)^2 R_{\text{eff}}(t, T) - A\Big(\delta(T - T_0) + \sigma(T^4 - T_0^4)\Big) \end{aligned} \tag{6}$$

and thus we obtain an effective memristive effect.

In order to estimate the frequency at which the thermistor effect is negligible, we use the equation above. The estimate is independent from many-body effects, and since the effective resistance of the sample depends on the resistivity linearly (while not on the topology) we can work with an effective model. The specific heat capacity of permalloy is $c_v = 0.124$ cal/g/Celsius, the density $\rho = 8.74$ g/cm^3. Also, it has been known for some time [52] that the electrical resistivity of permalloy is linear in temperature in the range 273–1000 Celsius, and nearly doubles in that interval (80% gain in resistivity). However, we are not aware of resistivity measurements for structures like ours. Given a certain initial condition for the resistance R_0, thermocouple experiments are consistent with a negative coefficient thermistor, which follows an equation

$$R(T) = R(T_0)e^{-C(1/T - 1/T_0)}, \tag{7}$$

with C. The total heat capacity can be written as $C = c_v \times V \times \rho$, where ρ is the density of the sample, and $V = A \times h$ is the volume, given by the area times the thickness.

In our experiment we can estimate that $R_0 \approx 720\Omega$ at $T_0 = 307$ K, and $R_1 \approx 755\Omega$ at $T_1 = 355$ K, from which we can estimate $\alpha \approx 10^{-3}$ K^{-1}. Also, we neglect the radiative transport, since it is orders of magnitude smaller than the dissipation due to transfer of energy via the plate.

In order to make the equation adimensional, we divide by the room-temperature energy, $E_r = \kappa T_r$. If we define

$$w_T = \frac{T}{T_r}, \tag{8}$$

we can write

$$\frac{\partial w_T}{\partial t} = \frac{i(t)v(t)}{CT_r} - \frac{A\delta}{C}(w_T - w_0) \tag{9}$$

and writing explicitly C and $i(t)$ in terms of the area and the resistance explicitly, we obtain

$$\begin{aligned} \frac{\partial w_T}{\partial t} &= \frac{v^2(t)}{Ac_v mhT_r R_0[1 + T_r\alpha_T(w_T - w_0)]} \\ &\quad - \frac{\delta}{c_v h\rho}(w_T - w_0), \end{aligned} \tag{10}$$

and where we use

$$R(w_T) = R_0[1 + T_r\alpha_T(w_T - w_0)], \tag{11}$$

with $w_0 = T_0/T_r$; thus, if we choose T_0 to be room temperature, then $w_0 = 1$. For practical purposes, we can set $T_r\alpha \approx 0.3$. Now, we note that $1/\tau = \delta/c_v h\rho$ is a relaxation timescale, while $Ac_v\rho hT_r R_0 = \tau_v^{-1}\bar{v}^2$ is an effective activation voltage per unit of time, which depends on the area of the permalloy sample in contact with the surface. This implies that the smaller the area the more pronounced the memristive effect due to the temperature will be. This is one of the reasons why this effect is typically negligible in thin films, while it is more pronounced in our sample. Let us assume that the thermistor is near the equilibrium. What we are interested in is the interplay between the decay and the forcing and the relationship in terms of ω. We thus neglect the w dependence on the denominator of the voltage-forcing term.

The solution of the differential equation in this regime, and assuming that $v(t) = V_0\cos(\omega t)$ is given by

$$\begin{aligned} w_T(t) &= c_1 e^{-t/\tau} \\ &\quad + \frac{2\tau^2 V_0^2\omega\sin(2t\omega) + \tau V_0^2\cos(2t\omega)}{2\bar{v}^2\left(4\tau^2\omega^2 + 1\right)} \\ &\quad + \frac{\tau V_0^2\cos(2t\omega) + \left(4\tau^2\omega^2 + 1\right)\left(\tau V_0^2 + 2\bar{v}^2 w_0\right)}{2\bar{v}^2\left(4\tau^2\omega^2 + 1\right)}, \end{aligned} \tag{12}$$

where c_1 is the constant of integration given the initial condition, which however we see goes to zero exponentially fast. As a result, from the oscillations around equilibrium, we can estimate in a linear response regime the value of $\bar{v}$. Since in our experiments we do not see a strong decay or thermalization, we expect τ to be of order $\tau \sim 1 - 10$ s. Let us thus assume first that $\tau\omega \ll 1$. In this case, we have

$$\Delta w_T(t) = \frac{V_0^2}{\tau_v\bar{v}^2}\omega\tau^2\sin(2\omega t). \tag{13}$$

Since we observe that the oscillations in resistance are of order $\Delta R/R \approx 0.03$, we obtain a rough estimate for $\bar{v}$ in

the mHz of $\Delta w/3 \approx 0.03$ at $V_0 = 10$ V. We have

$$\frac{V_0^2 \omega \tau^2}{3 \times 0.03} \approx \tau_v \bar{v}^2. \tag{14}$$

Substituting these, we obtain an estimate for τ_v:

$$\tau_v \bar{v}^2 \approx 11.1\ [V]^2[s], \tag{15}$$

which, setting $\tau_v = 1$ as a unit of time, leads to an effective voltage necessary to observe a noticeable response in the frequency regime of our experiments of $\bar{v} = V_0 \approx 3.33$ V. This is indeed consistent with the experimental results.

On the other hand, in the regime, $\omega \gg \tau^{-1}$, we have, up to the first order in $1/\omega$

$$w_T(t) = \frac{\tau V_0^2 + 2\bar{v}^2 \tau_v w_0}{2\bar{v}^2 \tau_v} + \frac{1}{\omega} \frac{2\tau^2 V_0^2}{2\bar{v}^2 \tau_v \tau^2} \sin(2t\omega) + O\left(\frac{1}{\omega^2}\right)$$

from which we see that while the equilibrium depends on τ, the oscillations do not. We obtain

$$\Delta w_T(t) = \frac{1}{\omega} \frac{V_0^2}{\tau_v \bar{v}^2} \sin(2t\omega). \tag{16}$$

The result above means that if we increase the frequency ω by K, these should be suppressed by a factor $1/K$. This argument suggests that if we observe a memristive effect in *centihz* or *millihz* due to the thermal changes, these should be suppressed by a factor $10^{-8} : 10^{-9}$ in Ghz, and are thus negligible.

As a last comment, we now discuss why in thin films this effect is not usually observed, as we also found out in our experiments. The surface of the sample is roughly 25 mm^2, or 25×10^{-6} m^2. We prepare two samples, one with a sphere of 1 μm and 500 nm diameter. In the 500-nm sample, we can perform the calculation by directly assuming a certain density of holes. In an area of $A_f = 2.3 * 10^{-11}$ m^2 we have roughly 110 spheres, give or take. This implies that we itch out from the surface an area $A_i = 110 * \pi * (0.25 * 10^{-6})^2$, and thus we obtain a remaining area $A_s = A_f - A_i = 1.4 * 10^{-12}$ m^2. The ratio between $A_f / A_s \approx 16$, which implies that the effective activation voltage per unit of second of the thin film is given by

$$\frac{\bar{v}^2_{\text{itched}}}{\bar{v}^2_{\text{thin film}}} = \frac{1}{16}, \tag{17}$$

or 4 $\bar{v}_{\text{itched}} = \bar{v}_{\text{thin film}}$. The effect is thus at least one order of magnitude smaller in a thin-film permalloy. This implies that voltages of at least approximately equal to 30 V would be necessary to fully appreciate the memory effect, which is prohibitive without burning the sample.

In conclusion of the model above, we obtain that the thermistor controlled at a certain frequency ω has two regimes for the change of resistance per unit of time:

(a) $\omega\tau \ll 1$: the time evolution of the system leads to a oscillatory regime around the mean, with

$$\Delta R/T \approx \frac{R_0 V_0^2}{\tau_v \bar{v}^2} \omega \tau^2 \sin(2\omega t).$$

(b) $\omega\tau \gg 1$: a solution of the dynamics leads to a change in amplitude, given by

$$\Delta R/T \approx \frac{R_0 V_0^2}{\tau_v \bar{v}^2 \omega} \sin(2\omega t).$$

Again, since in our experiments we do not observe a strong decay or relaxation, we expect the relaxation time to be of the order of the seconds. We are thus in the first of the two regimes, which is what we use to estimate $\tau_v \bar{v}^2$, which is approximately of 3.3. Thus, we obtain the result that at slow frequencies the system is dominated by thermal effects. This is one of the reasons explaining why in our experiments we do have little dependence of the hysteresis curve on an applied field. Yet, as we show above, for larger frequencies' resistance memory oscillations are suppressed by a factor $1/\omega$. This implies that at higher frequencies we have a crossover effect between the thermal and the magnetic degrees of freedom in the material, which we characterize next in simulations.

B. Magnetization dynamics

In a previous work it was argued that when a current is run through the kagomé permalloy, the total resistance is finely controlled by the direction of magnetization of the wires [35,36,38]. It was shown [38] that the effect of the magnetoresistance is due to the presence of the vertices, where domain walls form, and the system can thus be interpreted as an electrical circuit with voltage drops at the vertices. In Ref. [39] it has been noted instead that such a construction can be mapped to a resistor network with voltage generators in series, and thus can be written in an analytical form and mapped to an effective memristive effect.

More recently, it has been shown that in magnetic nanorings, the interplay between AMR and the Zhang-Li coupling are sufficient for the ring to exhibit memristive effects, which are strongly dependent on the internal magnetization states [40]. As we see here, magnetic permalloy patterned as a kagomé lattice shows a residual memristive effect (on top of the bulk thermistor effect), which is magnetic in nature. We wish to show here that such an effect can in principle be attributed to a many-body phenomenon, which we attempt to qualitatively account for here.

As discussed in Ref. [39], for heterostructures such as a kagomé-patterned permalloy, the interplay between the AMR and the local magnetization of the structure can affect the resistivity of the material. Here we go beyond the spinlike approximation used in Ref. [39] and study the magnetization reversal in a realistic model. Specifically, magnetization reversal processes in kagomé nanowires are verified by micromagnetic simulations based on the open-source GPU-based software MUMAX^3.

From energy minimization, one obtains sequences of snapshots between spin configurations, which are based on the Landau-Lifshitz-Gilbert (LLG) equation with the spin-transfer torque [53],

$$\frac{\partial \mathbf{M}}{\partial t} = \gamma \mathbf{H}_{\text{eff}} \times \mathbf{M} + \frac{\alpha}{M_S}\mathbf{M} \times \frac{\partial \mathbf{M}}{\partial t} - u\frac{\partial \mathbf{M}}{\partial y} + \frac{\beta}{M_S}\mathbf{M} \times \frac{\partial \mathbf{M}}{\partial y}. \tag{18}$$

In simulations we use periodic boundary conditions on a lattice of 5×5 μm size and with finite-difference discretization for the iterations [following Eq. (18) with cubic cell of $5 \times 5 \times 5$ nm]. The numerical parameters we use are those of permalloy, for which later in this paper we perform the experiments. They are magnetic saturation $M_S = 860 \times 10^3$ A m^{-1}, exchange constant $A_{\text{ex}} = 13 \times 10^{-12}$ J m^{-1}, polarization $P = 0.5$, and Gilbert damping $\alpha = 0.01$ for dynamics. In simulations we introduce a density of current $J_y = 2 \times 10^{13}$ A/m^2, cycling at a frequency ω. The numerical calculations are carried by a second-order Heun's solver with a fixed time step of 1×10^{15} s [54].

To better understand the role of magnetization dynamics in the memristive effect in the $I \times V$ measurements performed in kagomé lattices, while an analysis of extended magnetic objects escapes a complete analytical treatment, the intuition for the behavior of electrical-magnetic interactions can be obtained via intense numerical scrutiny. For that purpose we have utilized micromagnetic simulations in samples without [Fig. 5(a)] and with [Fig. 5(b)] the presence of an applied 0.3-T constant magnetic field on the y axis.

In the frames of magnetization distribution taken in positions 1–5 during the current loop, one can see that in the lattice without external magnetic field two processes are present, domain-wall motion by the current, which is applied in the y direction, with nanowires' magnetization flip in the x direction (inset 1 and 2), aside from the periodic domain-wall creation and annihilation by the particular geometry of the borders for high currents [55].

Despite the many-body effect contribution to the memristive effect, analytically predicted in previous work [35], the asymmetric disorder brought by the periodic domain-wall creation between increasing (frame 2) and decreasing (frame 4) current regime is mainly responsible for the memristive effect observed. In the saturated regime under an external magnetic field, the many-body effect is not present as expected, however, the geometric anisotropy is strong enough to shift the magnetization in relation to the current polarization direction to achieve the condition for periodic domain-wall creation, then even in the saturation regime, the asymmetric disorder is observed (insets 3 and 4).

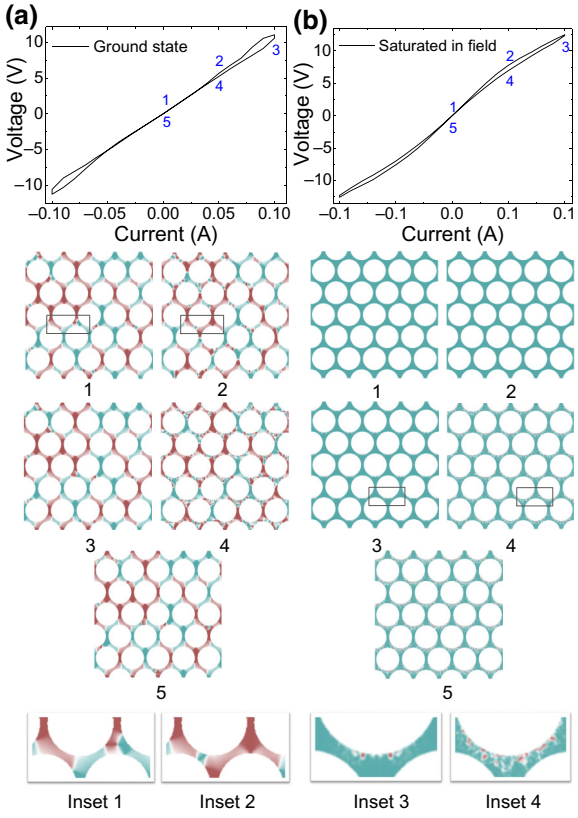

FIG. 5. (a) $I \times V$ curves obtained from micromagnetic simulation performed by spin-polarized current sweep in a sample with ground-state magnetization. Frames of magnetization states in points 1–5 of the loop are presented with an enlarged view in insets 1 and 2. (b) Same procedure performed in a sample with magnetization saturated by a magnetic field of 0.3 T.

IV. CONCLUSION

The present paper presents experimental investigation of the AMR-induced memristive effect in magnetic materials. We lithographically print (via colloidal deposition) a kagomé lattice of permalloy nanowires with two different lengths, and study the device memristive phenomenology in comparison with the thin film. The history dependence of the magnetization on the current is observed in the analysis of the anisotropic magnetoresistance, which has a higher signal in comparison with e-beam lithographed samples, due to the large area of vertex obtained. While

the bulk of the phenomenon can be explained via a thermistive effect not present in thin films, also confirmed via a thermocouple analysis, we find that 1% of the effect can be associated to the AMR-induced hysteresis.

In order to characterize the phenomenon, we study via micromagnetic simulations the effect of the current in the sample, and find that domain walls and spin waves can be found. However, thermal and dynamics effects can be removed by analyzing the difference between curves obtained in the experiments with and without external fields, and the many-body memristive characteristic can be measured.

While overall we do find that a residual effect can be attributed to a magnetic induced memristive effect, both in numerical simulations and experiments, the presence of the contribution of a thermistive effect prevents us from making precise statements on the nature of the phenomenon. This said, we do find good evidence that the combination of a coupling between the magnetization and the current via spin torque and anisotropic magnetoresistance leads to a polar memristive effect. Some comments are in order. It is interesting to note that the hysteresis curves of our experiments exhibit very little noise levels compared to other similar devices [31]. This is typically not the case for memristors, which have (again, typically) noise in the hysteresis curve.

Our numerical results and experiments suggest that tuning parameters, and using different materials, could allow domain-wall motion at lower currents. The theoretical analysis we perform on the thermistor also suggests that the thermistive effect should not be present at higher frequencies. Thus, experiments performed in the Ghz regime should eliminate spurious effects. Similarly to what is described for the case of magnetic rings [40], pure magnetically induced memristive effects should be present at that scale. We will discuss in future works the applications of our effective memristor in order to build networks of memristive devices [56,57].

ACKNOWLEDGMENTS

The financial support for this research is provided by the Brazilian agencies FINEP, FAPEMIG, and CAPES (Finance Code 001). The work of F.C. is carried out under the auspices of the U.S. Department of Energy through the Los Alamos National Laboratory, operated by Triad National Security, LLC (Contract No. 892333218NCA000001).

W.B.J.F. and F.G. designed and developed the samples. C.I.L.A. performed the experimental measurements and numerical simulations, and F.C. worked on the theoretical model. All authors contributed to discussing the experiments, the models to explain it, and writing the paper.

[1] C. Castelnovo, R. Moessner, and S. L. Sonhdi, Spin ice, fractionalization, and topological order, Annu. Rev. Condens. Matter Phys. **3**, 35 (2012).

[2] E. Mengotti, L. J. Heyderman, A. F. Rodríguez, F. Nolting, R. V. Hügli, and H. B. Braun, Real-space observation of emergent magnetic monopoles and associated Dirac strings in artificial kagome spin ice, Nat. Phys. **7**, 68 (2010).

[3] Y. Lao, F. Caravelli, M. Sheikh, J. Sklenar, D. Gardeazabal, J. D. Watts, A. M. Albrecht, A. Scholl, K. Dahmen, C. Nisoli, and P. Schiffer, Classical topological order in the kinetics of artificial spin ice, Nat. Phys. **14**, 723 (2018).

[4] G.-W. Chern and P. Mellado, Magnetic monopole polarons in artificial spin ices, Europhys. Lett. **114**, 37004 (2016).

[5] S. Gliga, A. Kákay, R. Hertel, and O. G. Heinonen, Spectral Analysis of Topological Defects in an Artificial Spin-Ice Lattice, Phys. Rev. Lett. **110**, 117205 (2013).

[6] C. Nisoli, R. Moessner, and P. Schiffer, Colloquium: Artificial spin ice: Designing and imaging magnetic frustration, Rev. Mod. Phys. **85**, 1473 (2013).

[7] R. F. Wang, C. Nisoli, R. S. Freitas, J. Li, W. McConville, B. J. Cooley, M. S. Lund, N. Samarth, C. Leighton, V. H. Crespi, and P. Schiffer, Artificial spin ice in a geometrically frustrated lattice of nanoscale ferromagnetic islands, Nature **439**, 303-6 (2006).

[8] S. D. Bader, Colloquium: Opportunities in nanomagnetism, Rev. Mod. Phys. **78**, 1 (2006).

[9] I. Gilbert, Y. Lao, I. Carrasquillo, L. O'Brien, J. D. Watts, M. Mann, C. Leighton, A. Scholl, C. Nisoli, and P. Schiffer, Emergent reduced dimensionality by vertex frustration in artificial spin ice, Nat. Phys. **12**, 162 (2016).

[10] L. J. Heyderman and R. L. Stamps, Artificial ferroic systems: Novel functionality from structure, interactions and dynamics, J. Phys.: Conden. Matter **25**, 363201 (2013).

[11] B. Canals, I. A. Chioar, V. D. Nguyen, M. Hehn, D. Lacour, F. Montaigne, A. Locatelli, T. O. Menteş, B. S. Burgos, and N. Rougemaille, Fragmentation of magnetism in artificial kagome dipolar spin ice, Nat. Commun. **7**, 11446 (2016).

[12] I. A. Chioar, N. Rougemaille, and B. Canals, Ground-state candidate for the classical dipolar kagome Ising antiferromagnet, Phys. Rev. B **93**, 214410 (2016).

[13] C. Nisoli, R. Wang, J. Li, W. F. McConville, P. E. Lammert, P. Schiffer, and V. H. Crespi, Ground State Lost but Degeneracy Found: The Effective Thermodynamics of Artificial Spin Ice, Phys. Rev. Lett. **98**, 217203 (2007).

[14] C. Nisoli, J. Li, X. Ke, D. Garand, P. Schiffer, and V. H. Crespi, Effective Temperature in an Interacting Vertex System: Theory and Experiment on Artificial Spin Ice, Phys. Rev. Lett. **105**, 047205 (2010).

[15] I. Gilbert, G. W. Chern, B. Fore, Y. Lao, S. Zhang, C. Nisoli, and Peter Schiffer, Direct visualization of memory effects in artificial spin ice, Phys. Rev. B **92**, 104417 (2015).

[16] P. E. Lammert, X. Ki, J. Li, C. Nisoli, D. M. Garand, V. H. Crespi, and P. Schiffer, Direct entropy determination and application to artificial spin ice, Nat. Phys. **6**, 786 (2010).

[17] F. Caravelli and C. Nisoli, Logical gates embedding in artificial spin ice, New J. Phys. 103052 (2022).

[18] H. Arava, P. M. Derlet, J. Vijayakumar, J. Cui, N. S. Bingham, A. Kleibert, and L. J. Heyderman, Computational logic with square rings of nanomagnets, Nanotechnology **29**, 265205 (2018).

[19] J. H. Hensen, E. Folven, and G. Tufte, Computation in artificial spin ice, Proc. of ALIFE 2018, p. 15, MIT Press, (2018).
[20] H. Dery, P. Dalal, Ł. Cywiński, and L. J. Sham, Spin-based logic in semiconductors for reconfigurable large-scale circuits, Nature **447**, 573 (2007).
[21] S. A. Wolf, D. D. Awschalom, R. A. Buhrman, J. M. Daughton, S. von Molnar, M. L. Roukes, A. Y. Chtchelkanova, and D. M. Treger, Spintronics: A spin-based electronics vision for the future, Science **294**, 1488 (2001).
[22] A. Ney, C. Pampuch, R. Koch, and K. H. Ploog, Programmable computing with a single magnetoresistive element, Nature **425**, 485 (2003).
[23] M. Patra and S. K. Maiti, All-spin logic operations: Memory device and reconfigurable computing, Europhys. Lett. **121**, 38004 (2018).
[24] Y. Zhang, Spintronics for Low-Power Computing, IEEE in Design, Automation and Test in Europe Conference and Exhibition, (2014),.
[25] F. L. Traversa, C. Ramella, F. Bonani, and M. Di Ventra, Memcomputing NP-complete problems in polynomial time using polynomial resources and collective states, Sci. Adv. **1**, e1500031 (2015).
[26] F. L. Traversa and M. Di Ventra, Polynomial-time solution of prime factorization and NP-complete problems with digital memcomputing machines, Chaos **27**, 023107 (2017).
[27] H. Manukian, F. L. Traversa, and M. Di Ventra, Memcomputing numerical inversion with self-organizing logic gates, IEEE Trans. Neural Netw. Learn Syst. **29**, 2645 (2017).
[28] F. Traversa and M. Di Ventra, Memcomputing: Leveraging memory and physics to compute efficiently, J. App. Phys. **123**, 180901 (2018).
[29] F. Caravelli, F. L. Traversa, and M. Di Ventra, Complex dynamics of memristive circuits: Analytical results and universal slow relaxation, Phys. Rev. E **95**, 022140 (2017).
[30] F. Caravelli, Asymptotic behavior of memristive circuits and combinatorial optimization, Entropy **21**, 789 (2019).
[31] F. Caravelli and J. P. Carbajal, Memristors for the curious outsiders, Technologies **6**, 118 (2018). engrXiv preprint:c4qr9.
[32] D. S. Jeong, K. M. Kim, S. Kim, B. J. Choi, and C. S. Hwang, Memristors for energy-efficient new computing paradigms, Adv. Electron. Mater. **2**, 1600090 (2016).
[33] T. Serrano-Gotarredon, T. Masquelier, T. Prodromakis, G. Indiveri, and B. Linares-Barranco, STDP and STDP variations with memristors for spiking neuromorphic learning systems, Front. Neurosci. **7**, 2 (2013).
[34] J. C. Gartside, K. D. Stenning, A. Vanstone, H. H. Holder, D. M. Arroo, T. Dion, F. Caravelli, H. Kurebayashi, and W. R. Branford, Reconfigurable training and reservoir computing in an artificial spin-vortex ice via spin-wave fingerprinting, Nat. Nanotechnol. **17**, 460 (2022).
[35] B. Le, J. Park, J. Sklenar, G.-W. Chern, C. Nisoli, J. Watts, M. Manno, D. Rench, N. Samarth, C. Leighton, and P. Schiffer, Understanding magnetotransport signatures in networks of connected permalloy nanowires, Phys. Rev. B **95**, 060405(R) (2017).
[36] T. R. McGuire and R. I. Potter, Anisotropic magnetoresistance in ferromagnetic 3d alloys, IEEE Trans. Magn. **11**, 1018 (1975).
[37] W. R. Branford, S. Ladak, D. E. Read, K. Zeissler, and L. F. Cohen, Emerging chirality in artificial spin ice, Science **335**, 1597 (2012).
[38] G.-W. Chern, Magnetotransport in Artificial Kagomé Spin Ice, Phys. Rev. Appl. **8**, 064006 (2017).
[39] F. Caravelli, G.-W. Chern, and C. Nisoli, Artificial spin ice phase-change memory resistors, New J. Phys. **24**, 023020 (2022).
[40] F. Caravelli, E. Iacocca, G.-W. Chern, C. Nisoli, and C. I. L. de Araujo, Anisotropic magnetomemristance, Commun. Phys. **5**, 166 (2022).
[41] D. B. Strukov, G. Snider, D. R. Stewart, and R. S. Williams, The missing memristor found, Nature **453**, 80 (2008).
[42] A. Yamaguchi, T. Ono, S. Nasu, K. Miyake, K. Mibu, and T. Shinjo, Real-Space Observation of Current-Driven Domain Wall Motion in Submicron Magnetic Wires, Phys. Rev. Lett. **92**, 077205 (2004).
[43] S. Krishnia, I. Purnama, and W. S. Lew, Observation of ice-rule violation and monopole dynamics via edge nucleation of domain walls in artificial spin ice lattice, J. Mag. Mag. Mater. **420**, 158 (2016).
[44] N. Vernier, D. A. Allwood, D. Atkinson, M. D. Cooke, and R. P. Cowburn, Domain wall propagation in magnetic nanowires by spin-polarized current injection, Europhys. Lett. **65**, 526 (2004).
[45] A. Pushp, T. Phung, C. Rettner, B. P. Hughes, S. H. Yang, L. Thomas, and S. S. P. Parkin, Domain wall trajectory determined by its fractional topological edge defects, Nat. Phys. **9**, 505 (2013).
[46] S. Zhang and Z. Li, Roles of Nonequilibrium Conduction Electrons on the Magnetization Dynamics of Ferromagnets, Phys. Rev. Lett. **93**, 127204 (2004).
[47] J. M. Ginoux, B. Muthuswamy, R. Meucci, S. Euzzor, A. Di Garbo, and K. Ganesan, A physical memristor based Muthuswamy–Chua–Ginoux system, Sci. Rep. **10**, 19206 (2020).
[48] F. Burmeister, C. Schäfle, T. Matthes, M. Böhmisch, J. Boneberg, and P. Leiderer, Colloid monolayers as versatile lithographic masks, Langmuir **13**, 2983 (1997).
[49] Z. Yi, G. Niu, J. Luo, X. Kang, W. Yao, W. Zhang, Y. Yi, Y. Yi, X. Ye, T. Duan, and Y. Tang, Ordered array of Ag semishells on different diameter monolayer polystyrene colloidal crystals: An ultrasensitive and reproducible SERS substrate, Sci. Rep. **6**, 32314 (2016).
[50] A. Yamaguchi, H. Tanigawa, T. Ono, S. Nasu, K. Miyake, K. Mibu, and T. Shinjo, Effect of Joule heating in current-driven domain wall motion, Appl. Phys. Lett. **86**, 012511 (2005).
[51] R. P. Loreto, F. S. Nascimento, R. S. Gonçalves, J. Borme, J. C. Cezar, C. Nisoli, A. R. Pereira, and C. I. L. de Araujo, Experimental and theoretical evidences for the ice regime in planar artificial spin ices, J. Phys.: Condens. Matter **31**, 025301 (2018).
[52] M. V. Belous, V. G. Permyakov, and V. I. Popov, The electrical properties of thin permalloy films, Sov. Phys. J. **10**, 23 (1967).
[53] T. L. Gilbert, A Lagrangian formulation of the gyromagnetic equation of the magnetic field, Phys. Rev. **100**, 1243 (1955).

[54] J. Leliaert, J. Mulkers, J. De Clercq, A. Coene, M. Dvornik, and B. Van Waeyenberge, Adaptively time stepping the stochastic Landau-Lifshitz-Gilbert equation at nonzero temperature: Implementation and validation in MuMax3, AIP Adv. **7**, 125010 (2017).

[55] M. Sitte, K. Everschor-Sitte, T. Valet, D. R. Rodrigues, J. Sinova, and Ar. Abanov, Current-driven periodic domain wall creation in ferromagnetic nanowires, Phys. Rev. B **94.6**, 064422 (2016).

[56] F. Caravelli, Locality of interactions in memristive circuits, Phys. Rev. E **96**, 052206 (2017).

[57] F. Caravelli, The mise en scéne of memristive networks: Effective memory, dynamics and learning, Int. J. Par., Em. Dist. Sys. **33**, 350 (2018).